

Spray-Coated Multilayer Cellulose Nanocrystal—Chitin Nanofiber Films for Barrier Applications

Chinmay C. Satam,^{†,‡} Cameron W. Irvin,^{‡,‡} Augustus W. Lang,^{‡,‡} Jerel Cedric R. Jallorina,[†] Meisha L. Shofner,^{‡,‡} John R. Reynolds,^{§,‡,‡} and J. Carson Meredith^{*,†,‡,‡}

[†]School of Chemical and Biomolecular Engineering, Georgia Institute of Technology, 311 Ferst Drive NW, Atlanta, Georgia 30332, United States

[‡]School of Materials Science and Engineering, Georgia Institute of Technology, 771 Ferst Drive NW, Atlanta, Georgia 30332, United States

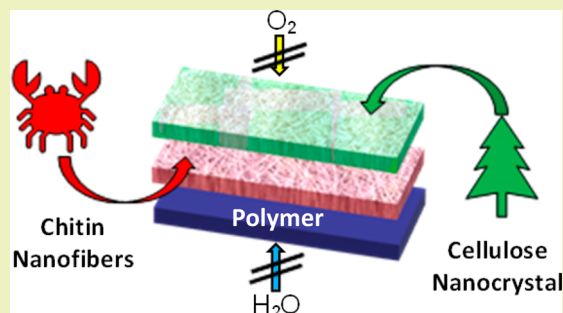
[§]School of Chemistry and Biochemistry, Center for Organic Photonics and Electronics, Georgia Tech Polymer Network, Georgia Institute of Technology, 901 Atlantic Drive, Atlanta, Georgia 30332, United States

[‡]Renewable Bioproducts Institute, Georgia Institute of Technology, 500 10th Street NW, Atlanta, Georgia 30332, United States

Supporting Information

ABSTRACT: Chitin is an abundant biopolymer whose natural production is second only to cellulose. Similar to cellulose nanocrystals (CNCs) or nanofibers (CNFs), chitin nanofibers (ChNFs) can be isolated and used as sustainable O₂ barrier materials for food, electronics, and pharmaceutical packaging. These bioavailable nanomaterials are readily dispersed in water enabling spray-coated films to be deposited at high rates onto uneven or delicate surfaces. In the present study, we demonstrate the successful layer-by-layer spray coating of cationic ChNF and anionic CNC suspensions onto poly(lactic acid) (PLA) films. ChNF/CNC multilayers were found to lead to a reduction in the O₂ permeability of the final composite film by as much as 73% with the largest effects seen in composites with three alternating layers (ChNF-CNC-ChNF). Multilayer ChNF/CNC coatings were found to have lower O₂ permeability and lower haze than those coated with ChNF or CNCs alone (72% and 86% lower haze, respectively), pointing to a synergistic effect. The composites had a water vapor transmission rate similar to the PLA substrate.

KEYWORDS: green materials, barrier materials, packaging materials, compostable, cellulose, chitin, layer-by-layer, renewable materials



INTRODUCTION

Cellulose and chitin are the first- and second-most abundant naturally occurring biopolymers, respectively, with annual natural production estimated to be 10¹¹–10¹² tons per year (cellulose)¹ and 10¹⁰–10¹² tons per year (chitin).² Cellulose is sourced most abundantly from plants, but it is also available from bacteria and tunicates. Chitin is produced by shellfish, insects, and fungi. Chemically, cellulose is a linear homopolymer of glucose and chitin is a linear homopolymer of N-acetyl glucosamine.³ In nature, chitin occurs as a copolymer in which some fraction of the acetamide groups on the 2 carbon are replaced by amine (–NH₂) groups. These amine groups can be protonated in acidic media to create charged sites that aid in the colloidal stabilization of chitin fibers, or complete solubilization with high degrees of deacetylation (as in the case of chitosan).

Both cellulose and chitin are found in hierarchical structures (in plant cell walls as well as crustacean exoskeletons, respectively), from which nanocrystals or nanofibers can be extracted. Because of their high crystallinity, cellulose nano-

crystals (CNCs), cellulose nanofibers (CNFs),^{4,5} chitin nanowhiskers, and chitin nanofibers (ChNFs)⁶ exhibit a high modulus and tensile strength and are excellent candidates for gas barrier films.^{7,8} The nanocrystalline or nanofibrous forms of these biopolymers represent promising renewable, compostable sources of materials for replacing traditional plastics in packaging applications. Typically, CNCs are produced by acid hydrolysis of a wide variety of fibrillar cellulose sources,⁴ while CNFs are produced by a mechanical defibrillation processes, which includes refining, homogenization, and grinding.⁹ In a manner similar to CNFs, when acidified chitin suspensions are subjected to high shear treatment, ChNFs of 10–20 nm diameter and several microns in length are obtained.^{6,8} Previously, Wu et al.⁸ produced chitin nanofibers in suspension from purified crab α -chitin. Suspension cast films were found to have O₂ and CO₂ gas permeabilities of 0.006 and 0.018

Received: May 1, 2018

Revised: June 16, 2018

barrer, respectively. In comparison, poly(ethylene terephthalate) (PET) has an O₂ permeability of 0.015–0.076 barrer¹⁰ and CO₂ permeability of 0.08–0.15 barrer.¹¹ This makes these chitin films excellent candidates in sustainable barrier packaging applications.

The inability to melt-process cellulose and chitin as neat materials is a principal obstacle to their use in packaging. However, the ease of suspending cellulose and chitin nanomaterials in water suggests their application as coatings to produce barrier films. Coatings allow fabrication of multilayered materials in an efficient manner, by combining multiple thin functional layers. A challenge of water processing of these materials is the low solids content at which high viscosity and gelation occur, which leads to the need to remove large quantities of water through drying. Rod coating¹² as well as slot-die coating¹³ have been used for coating CNF suspensions onto paperboard for barrier applications, taking advantage of the suspension's shear thinning behavior. Multilayered CNF films also have been prepared on silica substrates by using dip coating.¹⁴ Spin coating was also applied to coat CNC films on polypropylene¹⁵ and gas barrier properties of spin-coated multilayered CNC films have been reported.¹⁶

Spray coating is a versatile method for film deposition that offers enhanced drying rates because of the large surface area of droplets.¹⁷ One of the main features of spray coating is contactless delivery of material to the surface, allowing uneven or delicate surfaces to be coated.¹⁸ Beneventi et al.¹⁹ spray-coated slurries of microfibrillated cellulose onto wet, highly porous papers allowing complete retention of the microfibrillated cellulose on the surface of the substrate and improved barrier properties of the final product. Under sufficiently acidic conditions, ChNFs are cationic, and sulfate-modified CNCs are anionic. The opposite charges of chitin and cellulosic nanomaterials may facilitate their fabrication into multilayered barrier materials by promoting adhesion and rapid densification of their interfaces. For example, previous work by Qi et al.²⁰ successfully demonstrated layer-by-layer deposition of chitin nanofibers and TEMPO oxidized CNFs onto PET by using dip coating; however, the resulting films did not have improved barrier properties relative to uncoated PET. Park et al.²¹ successfully spray-coated aqueous chitosan solutions containing suspended clay to add barrier properties to poly(lactic acid) (PLA) films.

While PLA is a compostable polymer, PLA formulations typically suffer from the lack of cost-effective compostable additives. Thus, current efforts are being focused on producing partially renewable PLA-based materials.²² CNCs²³ and ChNFs²⁴ are renewable alternatives for barrier property modification of PLA. The goal of the present study is to demonstrate that a fully biologically sourced multilayer barrier film can be fabricated through a process compatible with roll-to-roll coating, by using oppositely charged ChNFs and CNCs applied to a suitable model compostable substrate (PLA). Single and multiple layers of ChNFs and CNCs were spray-coated from their aqueous suspensions onto PLA. Film structure was analyzed by scanning electron microscopy (SEM), atomic force microscopy (AFM), and UV–vis spectroscopy. The resulting barrier and mechanical properties were determined, revealing an important synergy between CNCs and ChNFs that yielded enhanced O₂ barrier properties in their multilayered coatings compared to films composed solely of ChNFs or CNCs alone.

MATERIALS AND METHODS

Materials. All chemicals and gases were purchased from commercial suppliers and used without further purification unless otherwise noted. Crab shells were purchased from Neptune's Harvest (Gloucester, MA). Natureworks LLC (Minnetonka, MN, U.S.A.) 4032D PLA was extruded into films of 25.4 μm thickness. CNCs as a 5.5 wt % aqueous suspension were provided by the USDA Forest Products Laboratory (Madison, WI). The CNCs had 0.86 wt % sulfur content via sulfate functionality with Na⁺ counterions. The CNC suspension was diluted to 0.5 wt % by addition of deionized (DI) water. Additional experimental details can be found in the [Supporting Information](#).

Extraction of ChNFs. Crab shells were treated with sodium hydroxide to remove proteins and hydrochloric acid to remove minerals in a manner similar to previous literature⁸ to yield purified chitin. Full details are given in the Supporting Information ([Figure S1](#)). A 0.5 wt % purified chitin suspension was prepared in DI water. The pH of the suspension was adjusted to 3.0 using glacial acetic acid and the acidified suspension was homogenized in a Mini DeBEE Homogenizer (BEE International, South Easton, MA). The first sequence of homogenization was carried out at a pressure of 1034 bar by using a 0.2 mm nozzle for 20 passes followed by a second sequence at 1516 bar and utilizing a 0.13 mm nozzle for an additional 10 passes. The resulting suspension was then used for spray coating. Because of the fluid expansion through the nozzle resulting in shear heating, a product cooler was used throughout the processing to keep the ChNF suspension at a maximum temperature of 35 °C.

ChNF Characterization. The degree of acetylation (DA) of the chitin was determined by potentiometric titration. The O₂ permeability values of these neat films were obtained by using a MOCON OXTRAN 1/50 instrument at values of relative humidity (RH) ranging from 0 to 80%. The water vapor transmission rate (WVTR) of these films were obtained by using a MOCON PERMATRAN-W 1/50 instrument at values of RH ranging from 30 to 90%.

PLA Characterization. Water content of neat PLA films was found by thermogravimetric analysis (TGA) using a TA Instruments TGA Q50 ([Figure S3](#)). The glass transition temperature (*T_g*) ([Figure S4](#)) and percent crystallinity (from [Figure S5](#)) of the neat PLA films was obtained by differential scanning calorimetry (DSC) using a DSC Q200 from TA Instruments.

Spray Coating. The spray coating apparatus is shown in [Figure S6](#) and consists of a 1.52 mm spray nozzle (Central Pneumatic, GA) connected to a liquid reservoir containing a 0.5 wt % ChNF or 0.5 wt % CNC suspension. The nozzle was supplied with a carrier gas by connection to a nitrogen cylinder at 4 bar. The PLA film was fixed to a heated surface and held at 60 °C during spray coating. Each coating layer was deposited by spraying the PLA with a 30 mL volume of the ChNF or CNC suspension, with 2 min drying time allowed between subsequent coatings. As a control the procedure was repeated by spraying only DI water (no CNC or ChNF) onto the PLA film, henceforth referred to as uncoated PLA films.

Sprayed Film Characterization. Water content of coated PLA films was found in a similar manner to neat PLA films using TGA. Light transmission measurements were made by using a Cary 5000 UV–vis-NIR equipped with an integrating sphere attachment (DRA 2500). PLA and multilayer-coated films were measured using a diffuse/normal geometry (di:0°) with the sample in the transmission port. Optical haze was calculated according to the following equation per ASTM D1003:

$$\text{haze (\%)} = \left(\frac{T_4}{T_2} - \frac{T_3}{T_1} \right) \times 100 \quad (1)$$

where *T*₁, *T*₂, *T*₃, and *T*₄ are transmittance values integrated from 380–780 nm for four different sample configurations. *T*₁ and *T*₃ correspond to geometries without the sample in the transmission port as an instrument correction. *T*₂ corresponds to the total sample transmittance (diffuse and specular), whereas *T*₄ captures only the diffuse transmittance.

Films were cut with blades, and SEM (LEO 1530) was used to image the cross section. The thicknesses of the coatings were determined by analysis of the SEM images. An image of neat PLA is shown in Figure S7a. For each coating thickness, at least 10 measurements were done at different points on SEM images. AFM (Bruker Icon) was utilized to image the top surface of coated films. The size of structures on the coated films were measured by visual analysis of the AFM phase images. Film roughness was determined from the AFM images by using Bruker Nanoscope Analysis software.

The O₂ permeability values of the coated and uncoated PLA films were obtained as described for neat ChNF but at RH values from 10 to 90% RH. The WVTR of films was obtained similar to neat films but at 30 to 90% RH. The measurement errors for multilayered composites were estimated to be proportional to the magnitude of the reading and extrapolated from the measurement error for O₂ permeability of neat PLA at 50% RH. Mechanical properties of uncoated and coated films were determined for comparison by using a high-throughput mechanical characterization (HTMECH) instrument.²⁵ This instrument utilizes a hemispherical indenter to deform films biaxially normal to the film plane until failure. The deformation rate was 10 mm/s and 3 measurements were taken on each film sample by using a 1.2 mm diameter indenter with a length of 34 mm. Stress vs strain curves obtained from one sample of each type of coated or uncoated film are shown in Figure S9. The maximum of the stress strain curve is determined to be the ultimate tensile strength while the stress at break is determined to be the breaking strength of the material.

RESULTS AND DISCUSSION

To fabricate multilayer coatings, ChNFs were first spray coated directly onto the PLA, followed by alternating spray-coated layers of CNCs and ChNFs. In describing the multilayer films, we use the terminology PLA-(X)_n, where (X)_n describes either single layers or bilayers of material. Thus, a PLA film coated with a single layer of CNCs is described as PLA-(CNC)₁ while PLA coated with 5 alternating layers of ChNFs and CNCs, starting with ChNF first is written as PLA-(ChNF-CNC)₂-ChNF.

Cross-sectional SEM images were taken order to visualize the change in film thickness with each coating layer. The evolution of film thickness is shown in Figure 1. To within experimental uncertainty, the coating thickness increases with the increase in number of coated layers. The coating thickness for a multilayer PLA-(ChNF-CNC)₂-ChNF film increases to 3.7 μm while the coating thicknesses increases to 7.7 and 6.4 μm for PLA-(ChNF)₅ and PLA-(CNC)₅ films, respectively.

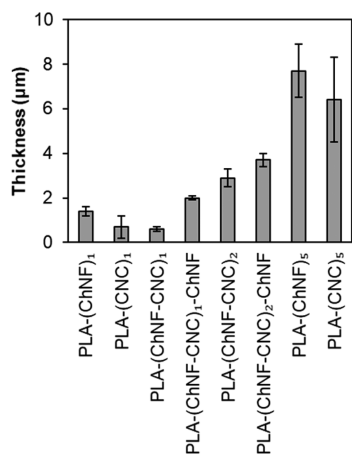


Figure 1. Film thicknesses of PLA films with and without single and multilayer coatings. Error ranges are 95% confidence intervals.

Thermal measurements of uncoated PLA using DSC gave the T_g of the neat PLA film as 63 °C and the crystallinity was 9.5%. The water content calculated from the TGA measurements for PLA-(CNC)₅, was 1.5 wt %, 0.9 wt % for and PLA-(ChNF)₅ films and 0.3 wt % for PLA. The DA of chitin as determined by potentiometric titration was found to be $92.6 \pm 2.8\%$.

The optical transmittance of neat and coated PLA films is summarized by the photographs, transmittance, and haze values shown in Figure 2. As shown in the photographs, the visible appearance of neat PLA (Figure 2a) and PLA-(CNC-ChNF)₁ (Figure 2b) films are similar, and the underlying colored patterns are clearly visible. The coated PLA-(ChNF-CNC)₁ has a matte finish due to its diffuse light reflection compared to the neat PLA. The optical transmittance for each film at 550 nm is shown Figure 2c where a slight decrease in % T is seen going from neat PLA (92.7%T) to the multilayer coated-PLA (91%T). The PLA-(CNC)₅ sample shows a notably decreased transmittance (88.3%) because of a large amount of scattering in the sample. The haze of each film was calculated using eq 1 and is shown in Figure 2d. The addition of a single spray-cast layer onto PLA increases the haze from 0.8% to 2.7% (ChNF) or 6.9% (CNC).

Interestingly, the film haze does not increase with additional layers. The 5-layer sample (PLA-(ChNF-CNC)₂-ChNF) has a haze of 6.3% which is far lower than the haze of equivalent five layered films composed solely of ChNF (23%) and CNC (46%). The lower haze for multilayered films suggests that alternating the oppositely charged ChNFs and CNCs produces denser films with fewer voids to scatter light. Wagberg et al.²⁶ made smooth, well-organized multilayer films with CNF and polyelectrolytes (PEs). They concluded that during adsorption of the CNF to the PE surface, electrostatic repulsion between the fibrils prevents their aggregation and allows better organization into thin layers. The PE charge characteristics and solution ionic strength had a large influence on the

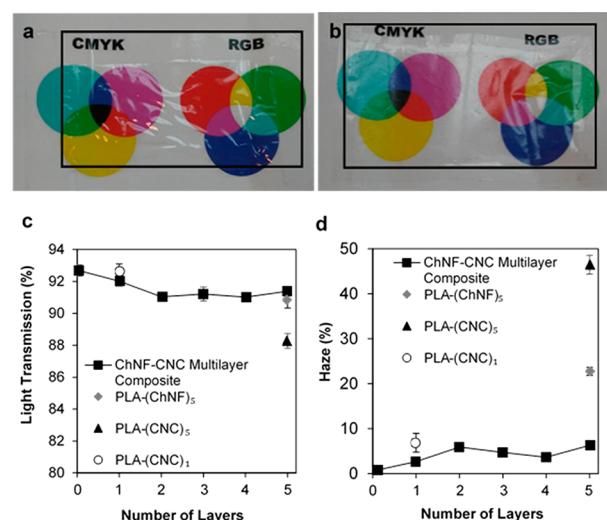


Figure 2. (a) Photos of neat PLA and (b) PLA-(CNC-ChNF)₁ films covering CMYK and RGB colored swatches. (c) Light transmission versus number of layers of films measured at 550 nm (d) Optical haze calculated over the visible spectrum (380–780 nm). Filled squares denote PLA (layer 0) coated with ChNF (layer 1), then CNC (layer 2), then (ChNF), and so on. The same convention is used in the remaining figures.

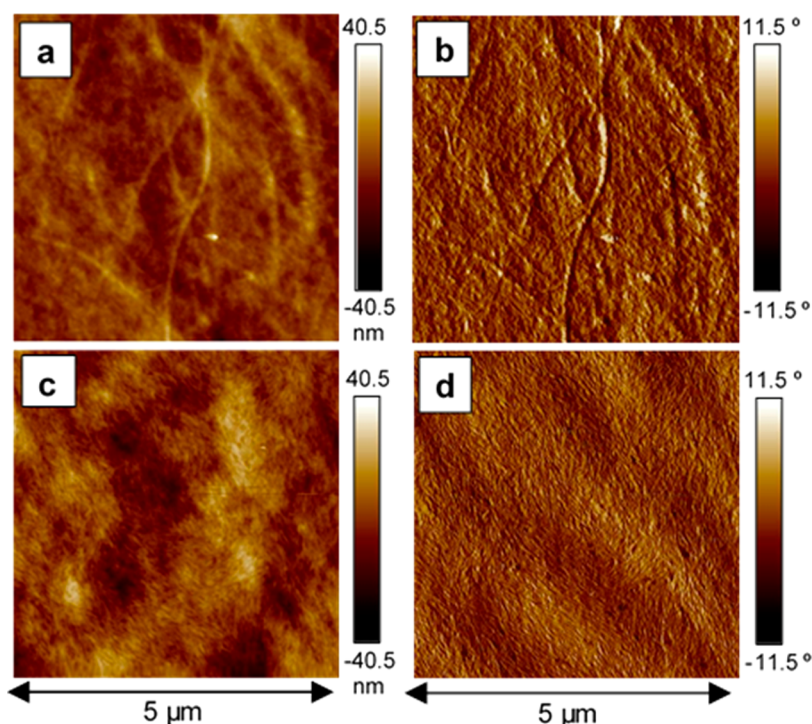


Figure 3. Representative AFM images of coated PLA films. (a) Height image and (b) phase image of top layer coating of ChNFs on a (PLA-(ChNF-CNC)₁-ChNF) multilayer; (c) height image and (d) phase image of top layer coating of CNCs on a (PLA-(ChNF-CNC)₂) multilayer.

thickness of CNF-PE multilayers. Increasing the PE solution ionic strength by salt addition caused an increase in layer thickness, indicating that packing was inefficient due to screening of long-range electrostatic interactions. In addition, PEs formed from weaker, less-charged bases produced thicker layers than stronger basic PEs. While the PEs are molecularly dissolved and the ChNFs are suspended particles, the similarities in charge characteristics between the two systems (CNF-PE and CNC-ChNF) are significant enough to warrant a comparison as long-range electrostatic forces are expected to be the most dominant forces in both systems. We expect that the attractive electrostatics between ChNFs and CNCs promotes strong adsorption of thin alternating layers, and that self-repulsion between ChNFs or CNCs in any layer allows each layer to pack more efficiently. It is known that the pK_a of sulfate ester group on CNCs is 2.46²⁷ as compared with that of acetic acid (used for homogenization of chitin), which is 4.76.²⁸ Thus, the deprotonated, negatively charged sulfonate groups on CNC would promote the adsorption of positively charged ChNFs on the CNC surface, and repulsive interactions between similarly charged ChNFs (or CNCs) would promote their rearrangement into more efficiently packed layers. This effect could produce thinner films with reduced voids in the light transmission path resulting in less light scattering.

AFM measurements were next used to visualize the surface density of particles in the multilayer films. In Figure 3a we see the height image of the top ChNF layer on (PLA-(ChNF-CNC)₁-ChNF). Figure 3b shows the corresponding phase image. Individual fibers can be seen on the surface, some of which are several microns in length. The fibers vary in diameter from 20 to 100 nm. It must be pointed out that fibers smaller than 20 nm will not be resolved in these images. Figure 3c shows the height image of the top CNC layer on (PLA-(ChNF-CNC)₂) with the phase image shown in Figure 3d. In these images, individual CNC whiskers are dried into a

compressed layer with ordered regions suggestive of formation of a nematic phase during drying. This is consistent with the known structural ordering of CNCs at semidilute concentrations.²⁹ The CNCs appear to be 150 ± 30 nm in length and have varying diameters of 20–60 nm. The typical Forest Products Lab CNCs from dissolving pulp are 150–200 nm in length and approximately 5 nm in diameter³⁰ suggesting clusters of longitudinally oriented CNCs.

The ChNF films have an average surface roughness of 11.8 ± 2.0 nm while the CNC films have a roughness of 7.2 ± 1.2 nm based on averages of 3 samples. The roughness of CNC films is consistent with the diameter of CNCs while the roughness of ChNFs is consistent with single ChNF fiber diameters as mentioned before. The ChNF fibers show much larger variation in fiber diameters which might lead to a higher surface roughness than CNCs, which are more uniform in size.

Film cross sections were imaged by SEM and analyzed to understand the evolution of film thickness with the number of layers in the coating. Figure 4 shows cross-sectional SEM images of PLA films coated with ChNFs, CNCs, or both in multilayers. The films with ChNF coating on the top (outermost) layer appear rougher than those with CNC as the top layer, which is consistent with the AFM images shown in Figure 3. In all cases, the films completely cover the underlying surface, except for the PLA-(ChNF)₅ and PLA-(CNC)₅ films where cracks can be seen in the layers. The transverse directional cracks suggest that these thick neat layers are brittle, and this may be related to the apparently lower density and drying pathway followed in the thick neat films. However, SEM-induced cracking artifacts cannot be excluded.

The reduction in coating thickness observed in going from PLA-(ChNF)₁ to PLA-(ChNF-CNC)₁ is unexpected. It has been observed that a *blended* mixture of 0.5 wt % ChNF and CNC suspensions produces thinner films than equivalent volumes of ChNFs and CNCs alone (Table S2). In the

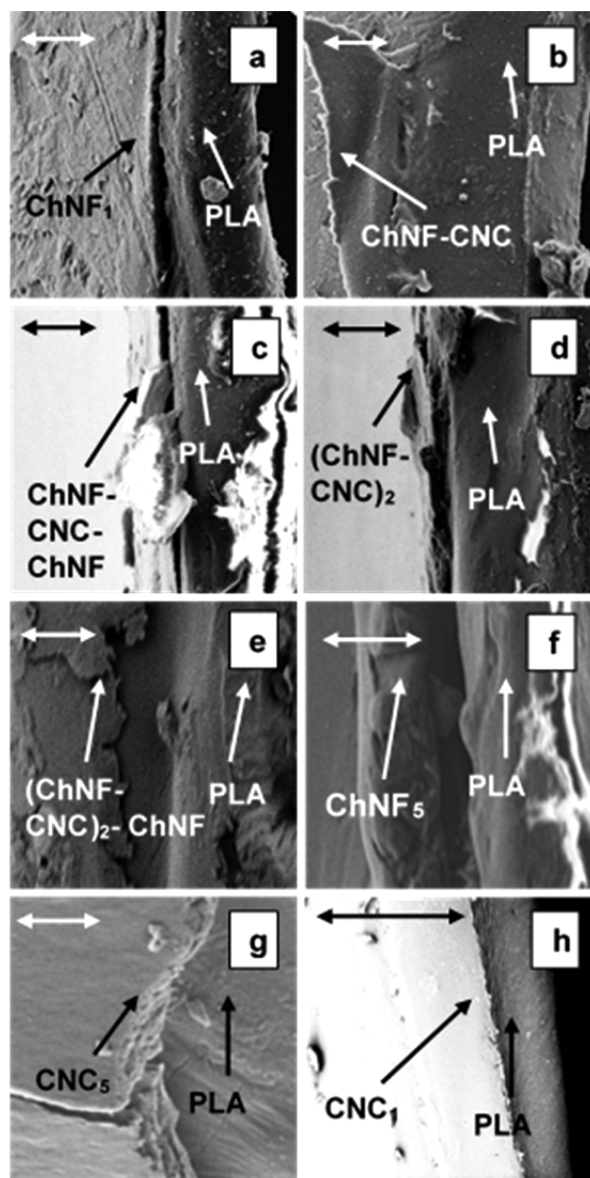


Figure 4. SEM cross-sectional images of fractured films: (a) PLA-(ChNF)₁, (b) PLA-(ChNF-CNC)₁, (c) PLA-(ChNF-CNC)₁-ChNF, (d) PLA-(ChNF-CNC)₂, (e) PLA-(ChNF-CNC)₂-ChNF, (f) PLA-(ChNF)₅, (g) PLA-(CNC)₅, (h) PLA-(CNC)₁. All scale bars are 10 μm in length.

multilayered films, rewetting of underlying ChNF layers by the next deposited CNC suspension may allow for some interfacial mixing of ChNFs and CNCs resulting in thinner mixed ChNF-CNC films. While this explanation is supported by the observations on blended films, we cannot rule out inaccuracy in measurement or in the deposited volume of ChNF or CNC as a possible cause for the small PLA-(ChNF-CNC)₁ film thickness. However, the thickness-corrected O₂ permeability of this sample is markedly lower than the single ChNF or CNC samples and is almost identical to that of the thicker multilayer films, indicating that the density and intrinsic transport properties of PLA-(ChNF-CNC)₁ are similar to subsequently deposited layers (discussed below with Figure 5). The five-layered PLA-(ChNF-CNC)₂-ChNF films are thinner than the PLA-(ChNF)₅ and PLA-(CNC)₅ films, which suggests denser packing when the films are fabricated from thin, alternating

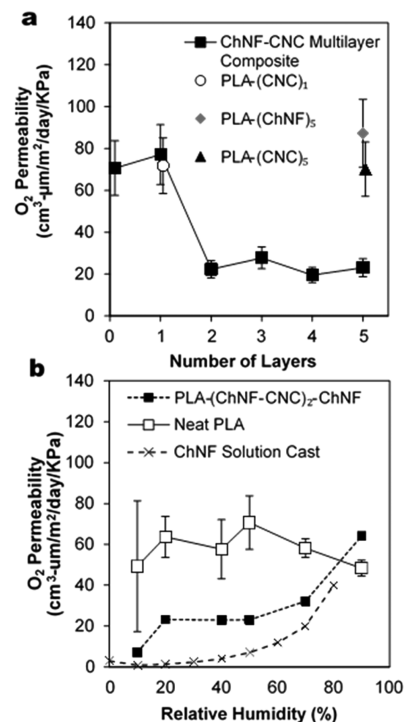


Figure 5. (a) O₂ permeability of PLA films with and without single and multilayer coatings of ChNFs and CNCs at 23 °C and 50% RH. (b) O₂ permeability versus RH of permeant gas at 23 °C.

multilayers compared to the equivalent sprayed volume of neat material.

The impact of this structure on the multilayer film's barrier properties was determined by measuring the oxygen permeability and the WVTR. Figure 5a shows the O₂ permeability of PLA films coated with ChNFs, CNCs, and alternating layers of ChNF and CNC measured at 50% RH. Upon coating with 1 ChNF layer, the film shows a slight increase in O₂ permeability from 70 to 80 cm³·μm/m²/day/kPa indicating that the first ChNF layer with a thickness of 1.4 μm does not improve barrier performance. The added ChNF instead increases the thickness of the composite material causing an increase in the effective permeability of the composite. This effect is also observed more dramatically in the thicker PLA-(ChNF)₅ films that are coated with 5 times the volume of ChNF suspension as the PLA-(ChNF)₁ film. For PLA-(ChNF-CNC)₁ films, the permeability drops to around 20 cm³·μm/m²/day/kPa, and adding additional alternating layers of ChNF and CNC, up to PLA-(ChNF-CNC)₅, results in essentially the same permeability. In comparison, a single 5-layer-equivalent of neat CNCs does not decrease the permeability significantly indicating that CNC coatings delivered as a single neat layer have roughly the same permeability as the neat PLA.

Figure 5b shows the O₂ transport characteristics of a PLA-(ChNF-CNC)₂-ChNF film as a function of RH. As RH increases, the oxygen transmission rate of coated PLA films increases in contrast to uncoated PLA films where the O₂ permeability remains in the range of 45–70 cm³·μm/m²/day/kPa without an obvious trend. The O₂ permeability of semicrystalline PLA has been reported by others to be between 95 and 115 cm³·μm/m²/day/kPa,³¹ while the permeability of amorphous PLA lies in between 130 and 190 cm³·μm/m²/day/kPa,³¹ which can change based on molecular

mass and processing history. These values are 2 to 4 times higher than the neat PLA utilized in this study, indicating that reductions in permeability reported here are conservative values.

The O_2 permeability of 10 μm thick neat solution-cast ChNF film also increases with an increase in RH as can be seen in Figure 5b. In addition, Aulin et al.³² showed that the O_2 permeability of cellulose nanofiber films increases with increasing RH. Belbekhouche et al.⁷ also reported higher permeability values for CNCs than CNFs and reported similar water vapor sorption isotherms for both materials. Therefore, it is reasonable to state that the O_2 transmission rates of CNC films in this work increase with RH and are at least as high as those reported for CNF films.³¹

At lower RH (<80%), the combined ChNF-CNC multilayers have a significantly lower O_2 permeability than the PLA alone and appear to control the O_2 permeability of the composite film. At higher RH, the O_2 permeability of the ChNF-CNC multilayer film approaches the range of permeability displayed by the neat PLA. This result indicates that the O_2 transmission is controlled by the PLA layer at RH exceeding 80%.

The WVTR of various barrier films is shown in Figure 6a. Multilayer films exhibit a WVTR in the range of 64–150 $\text{g}/\text{m}^2/\text{day}$, similar to neat PLA, even after coating with up to 5 alternating layers of ChNF and CNC. The WVTR of PLA-(CNC)₁ films also lies in the same WVTR range as neat PLA films. The WVTR of PLA-(ChNF)₅ films is similar to the multilayered films, but WVTR of PLA-(CNC)₅ is slightly higher than for PLA-(ChNF)₅. This is decidedly not due to off-gassing of water from the film as even PLA-(CNC)₅ and PLA-(ChNF)₅ films with the most amount of water sprayed on them due to higher spray coat volumes had less than 2 wt %

water. Figure 6b shows the WVTR characteristics as a function of RH for PLA, PLA-(ChNF-CNC)₂-ChNF, and a solution cast ChNF film. The multilayer film shows a slightly lower WVTR compared to neat PLA which increases in a similar fashion with RH. The WVTR of neat solution-cast ChNF film increases much more rapidly with RH compared to neat PLA. These two results indicate that the PLA controls the RH-dependence of WVTR for the PLA-(ChNF-CNC)₂-ChNF film. WVTR of neat CNF films has been reported to be around 230 $\text{g}/\text{m}^2/\text{day}$ for a 42 μm film at 50% RH and 23 $^\circ\text{C}$,³³ which after normalizing for thickness is 9800 $\text{g}\ \mu\text{m}/\text{m}^2/\text{day}$ and is similar to the 11 400 $\text{g}\ \mu\text{m}/\text{m}^2/\text{day}$ found for ChNFs here. Similar adjusted WVTR values were obtained for CNF films as reported by Bedane et al.³⁴ as well as by Nair et al.^{35,36} These results suggest that the ChNF-CNC multilayers have a much higher water vapor permeability than PLA and thus the PLA layer controls the transport of water in the composite as can be seen in Figure 6a. In summary, the composites have an O_2 permeability that is controlled by the ChNF-CNC coating and a WVTR that is controlled by the underlying PLA layer.

Ultimate tensile strength (UTS) and breaking strength were evaluated for films under biaxial strain by using an instrumented hemispherical indenter. The results summarized in Figure 7 show that upon adding layers of ChNFs or CNCs, both the UTS and breaking strength decrease with a dramatic loss of strength for the 5 layer coated films (PLA-(ChNF)₅, PLA-(CNC)₅, and PLA-(ChNF-CNC)₂-ChNF). Figure 7c shows that the strain at break initially decreases after adding one layer of ChNF in PLA-(ChNF)₁ but increases again with subsequent layering of CNCs, until 5 layers are reached where it decreases sharply. For each of the coated materials, the UTS and breaking strengths are similar indicating that the materials break close to their maximum tensile stress (UTS). The PLA-

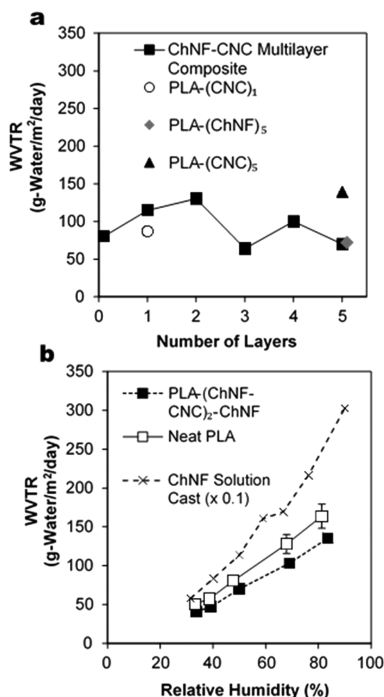


Figure 6. (a) WVTR of PLA films with and without single and multilayer coatings of ChNFs and CNCs at 23 $^\circ\text{C}$ and 50% RH. Measurement errors at 50% RH smaller than 7 $\text{g}\text{-water}/\text{m}^2/\text{day}$. (b) WVTR versus RH of permeant gas at 23 $^\circ\text{C}$.

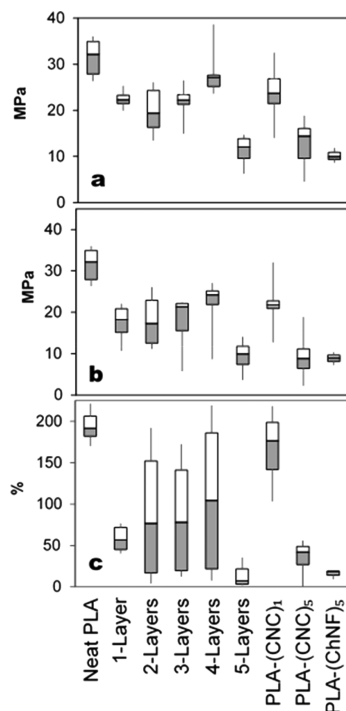


Figure 7. (a) UTS, (b) breaking strength, and (c) strain at break of coated and uncoated PLA films deformed biaxially with an instrumented probe.

(ChNF)₁ films behave similarly to the PLA-(CNC)₁ films as evidenced by similar breaking strength and UTS, but the PLA-(CNC)₁ films have a higher strain at break.

To understand the reduction in mechanical strength and strain at break of multilayered films, it is useful to consider that the mechanical attachment of two different materials may lead to stress concentrations that can initiate cracks at the interface.³⁷ There is a significant mismatch in thermal and mechanical properties at the interface of PLA and ChNF/CNCs. For example, the neat PLA films have a high strain at break of about 200%. Solution cast 0.5 wt % ChNF and CNC films were found to have a much lower strain at break ranging from 10–50% and 0.5–3% respectively, indicating that ChNF and CNC films are more brittle than neat PLA. Thermal contraction during cooling and volumetric contraction during drying of ChNFs and CNCs is expected to result in large residual stresses at the interface of ChNF and PLA. Such stresses are known to adversely affect mechanical integrity.³⁸ Another reason multilayered materials may fail at a lower strain and tensile strength than their parent materials is due to “mutual interlayer destruction.” In this type of failure, a brittle layer cracks first and this crack then acts as a notch to localize the stresses in an adjacent ductile layer, causing premature failure of the ductile material, leading to failure of the whole composite.^{39,40} Youngblood et al.⁴¹ reported reduced UTS, lower Young’s modulus and higher strain at break in (compared to neat CNF films) CNF-polymer laminates, while they reported reduction in all of these properties in CNC-polymer laminates.

All of the five-layered films in Figure 7 are similar in UTS and breaking strength, suggesting similarity in the effects of interfacial mismatch or brittleness above a threshold thickness. This is similar to embrittlement induced by high loads of neat polystyrene coextruded over high-impact (rubber-roughened) polystyrene, which fail due to mutual interlayer destruction.⁴⁰ Thus, a trade-off exists between barrier versus mechanical effects, suggesting that the number of brittle ChNF/CNC layers should be kept to a minimum required to achieve desired transport properties.

CONCLUSIONS

This study provides an initial perspective of the potential for utilizing alternating layers of chitin and cellulose-based nanofibrous materials to tune barrier properties. Multilayered coatings consisting of alternating layers of ChNFs and CNCs can be applied to PLA films through spray coating of the charge-stabilized aqueous suspensions of each material. This process can be considered a type of layer-by-layer coating process, where the CNCs are negatively charged and the ChNFs are positively charged. We found that spraying onto a heated substrate (60 °C, just under the glass transition for PLA) facilitated drying of the sprayed coatings before significant dewetting of the aqueous suspension occurred on the PLA film. We found that films with at least two alternating coated layers, consisting of PLA-(CNC-ChNF)_n, showed reductions in O₂ permeability relative to neat PLA, even at elevated RH (70%). Interestingly, these improvements in O₂ barrier properties were not observed for films with single layers of neat ChNF or CNC sprayed from an equivalent volume. The improvement in O₂ permeability was correlated with SEM and AFM evidence of thin, densely packed layers of ChNF and CNC. The composites were more brittle than neat PLA possibly due to mutual interlayer destruction, which could be

addressed by minimizing the thickness of coated layers or the use of plasticizers to decreasing the brittleness of the coated ChNF-CNCs. In terms of engineering applications, these films could form the basis for a platform technology of 100% biorenewable barrier packaging. A challenge to this goal that will form the basis of future work is the need to make improvements in WVTR, which was not intrinsically improved through the addition of ChNF or CNC layers (but continued to be controlled by the PLA film substrate). This technology can be applied to a variety of applications where oxygen permeability is a key problem, including packaging of foods, pharmaceuticals and electronics.

ASSOCIATED CONTENT

Supporting Information

The Supporting Information is available free of charge on the ACS Publications website at DOI: 10.1021/acssuschemeng.8b01536.

Complete materials, methods, and additional results (PDF)

AUTHOR INFORMATION

Corresponding Author

*E-mail: carson.meredith@chbe.gatech.edu. Phone: 404-385-2151.

ORCID

John R. Reynolds: 0000-0002-7417-4869

J. Carson Meredith: 0000-0003-2519-5003

Author Contributions

The manuscript was written through contributions of all authors. All authors have given approval to the final version of the manuscript.

Notes

The authors declare no competing financial interest.

ACKNOWLEDGMENTS

We are grateful for financial support from the Renewable Bioproducts Institute, Georgia Institute of Technology, Atlanta, GA. We would also like to thank Wei Liu and Professor Yulin Deng for their technical reviews and support as part of a larger IGER project. We would like to thank Frito Lay Inc., for their contributions to this work, including supply of extruded PLA material.

ABBREVIATIONS

CNC, cellulose nanocrystals; ChNF, chitin nanofibers; PLA, poly(lactic acid); CNF, cellulose nanofibers; PET, poly(ethylene terephthalate); SEM, scanning electron microscope; AFM, atomic force microscope; UV, ultraviolet; Vis, visible; TEMPO, 2,2,6,6-Tetramethylpiperidinyloxy; DI, deionized; DA, degree of acetylation; TGA, thermogravimetric analysis; RH, relative humidity; WVTR, water vapor transmission rate; DSC, differential scanning calorimetry; NIR, near-infrared; HTMECH, high-throughput mechanical characterization; PE, polyelectrolyte; CMYK, cyan magenta yellow key; RGB, red green blue; UTS, ultimate tensile strength.

REFERENCES

- (1) Klemm, D.; et al. Cellulose. In *Biopolymers in 10 volumes (volume 6 Polysaccharides II: Polysaccharides from Eukaryotes)*; De Baets, S., Vandamme, E., Steinbüchel, A. T., Eds.; Wiley-VCH: Germany, 2004.

- (2) Barikani, M.; Oliaei, E.; Seddiqi, H.; Honarkar, H. Preparation and application of chitin and its derivatives: a review. *Iran. Polym. J.* **2014**, *23*, 307–326.
- (3) Hamed, I.; Özogul, F.; Regenstein, J. M. Industrial applications of crustacean by-products (chitin, chitosan, and chitooligosaccharides): A review. *Trends Food Sci. Technol.* **2016**, *48*, 40–50.
- (4) Moon, R. J.; Martini, A.; Nairn, J.; Simonsen, J.; Youngblood, J. Cellulose nanomaterials review: structure, properties and nanocomposites. *Chem. Soc. Rev.* **2011**, *40*, 3941–3994.
- (5) Zimmermann, T.; Pohler, E.; Geiger, T. Cellulose fibrils for polymer reinforcement. *Adv. Eng. Mater.* **2004**, *6* (9), 754–761.
- (6) Ifuku, S.; Saimoto, H. Chitin nanofibers: preparations, modifications, and applications. *Nanoscale* **2012**, *4*, 3308–3318.
- (7) Belbekhouche, S.; Bras, J.; Siqueira, G.; Chappey, C.; Lebrun, L.; Khelifi, B.; Marais, S.; Dufresne, A. Water sorption behavior and gas barrier properties of cellulose whiskers and microfibrils films. *Carbohydr. Polym.* **2011**, *83* (4), 1740–1748.
- (8) Wu, J.; Zhang, K.; Girouard, N.; Meredith, J. C. Facile Route to Produce Chitin Nanofibers as Precursors for Flexible and Transparent Gas Barrier Materials. *Biomacromolecules* **2014**, *15* (12), 4614–4620.
- (9) Zhao, Y.; Moser, C.; Lindstrom, M. E.; Henriksson, G.; Li, J. Cellulose Nanofibers from Softwood, Hardwood, and Tunicate: Preparation-Structure-Film Performance Interrelation. *ACS Appl. Mater. Interfaces* **2017**, *9* (15), 13508–13519.
- (10) Lange, J.; Wyser, Y. Recent Innovations in Barrier Technologies for Plastic Packaging – a Review. *Packag. Technol. Sci.* **2003**, *16* (4), 149–158.
- (11) Massey, L. K. *Permeability Properties of Plastics and Elastomers: A Guide to Packaging and Barrier Materials*, 2nd ed.; William Andrew Publishing: Norwich, NY, 2002.
- (12) Mazhari Mousavi, S. M.; Afra, E.; Tajvidi, M.; Bousfield, D. W.; Dehghani-Firouzabadi, M. Cellulose nanofiber/carboxymethyl cellulose blends as an efficient coating to improve the structure and barrier properties of paperboard. *Cellulose* **2017**, *24* (7), 3001–3014.
- (13) Kumar, V.; Elfving, A.; Koivula, H.; Bousfield, D.; Toivakka, M. Roll-to-Roll Processed Cellulose Nanofiber Coatings. *Ind. Eng. Chem. Res.* **2016**, *55* (12), 3603–3613.
- (14) Aulin, C.; Johansson, E.; Wågberg, L.; Lindström, T. Self-Organized Films from Cellulose I Nanofibrils Using the Layer-by-Layer Technique. *Biomacromolecules* **2010**, *11* (4), 872–882.
- (15) d'Eon, J.; Zhang, W.; Chen, L.; Berry, R. M.; Zhao, B. Coating cellulose nanocrystals on polypropylene and its film adhesion and mechanical properties. *Cellulose* **2017**, *24* (4), 1877–1888.
- (16) Herrera, M. A.; Mathew, A. P.; Oksman, K. Gas permeability and selectivity of cellulose nanocrystals films (layers) deposited by spin coating. *Carbohydr. Polym.* **2014**, *112* (Supplement C), 494–501.
- (17) McKeen, L. W. *Application of Liquid Coatings Fluorinated Coatings and Finishes Handbook*; William Andrew Publishing: Norwich, NY, 2015.
- (18) Czerwonatis, N. Spray Coating—A Contactless Coating Process for Paper Finishing. *Proceedings of the TECH 31 Tape Summit*, Baltimore, Maryland, May 7–9, 2008; Pressure Sensitive Tape Council: Oakbrook Terrace, IL, 2008.
- (19) Beneventi, D.; Chaussy, D.; Curtil, D.; Zolin, L.; Gerbaldi, C.; Penazzi, N. Highly Porous Paper Loading with Microfibrillated Cellulose by Spray Coating on Wet Substrates. *Ind. Eng. Chem. Res.* **2014**, *53*, 10982–10989.
- (20) Qi, Z. D.; Saito, T.; Fan, Y.; Isogai, A. Multifunctional coating films by layer-by-layer deposition of cellulose and chitin nanofibrils. *Biomacromolecules* **2012**, *13* (2), 553–558.
- (21) Park, S. H.; Lee, H. S.; Choi, J. H.; Jeong, C. M.; Sung, M. H.; Park, H. J. Improvements in barrier properties of poly(lactic acid) films coated with chitosan or chitosan/clay nanocomposite. *J. Appl. Polym. Sci.* **2012**, *125* (S1), E675–E680.
- (22) Nagarajan, V.; Mohanty, A. K.; Misra, M. Perspective on Polylactic Acid (PLA) based Sustainable Materials for Durable Applications: Focus on Toughness and Heat Resistance. *ACS Sustainable Chem. Eng.* **2016**, *4* (6), 2899–2916.
- (23) Zhang, Z.; Wu, Q.; Song, K.; Ren, S.; Lei, T.; Zhang, Q. Using Cellulose Nanocrystals as a Sustainable Additive to Enhance Hydrophilicity, Mechanical and Thermal Properties of Poly(vinylidene fluoride)/Poly(methyl methacrylate) Blend. *ACS Sustainable Chem. Eng.* **2015**, *3* (4), 574–582.
- (24) Li, M.; Wu, Q.; Song, K.; Cheng, H. N.; Suzuki, S.; Lei, T. Chitin Nanofibers as Reinforcing and Antimicrobial Agents in Carboxymethyl Cellulose Films: Influence of Partial Deacetylation. *ACS Sustainable Chem. Eng.* **2016**, *4* (8), 4385–4395.
- (25) Sormana, J. L.; Chattopadhyay, S.; Merideth, J. C. High-throughput mechanical characterization of free-standing polymer films. *Rev. Sci. Instrum.* **2005**, *76* (6), 062214.
- (26) Wagberg, L.; Decher, G.; Norgren, M.; Lindstrom, T.; Ankerfors, M.; Axnas, K. The build-up of polyelectrolyte multilayers of microfibrillated cellulose and cationic polyelectrolytes. *Langmuir* **2008**, *24* (3), 784–795.
- (27) Ehmman, H.; Mohan, T.; Koshanskaya, M.; Scheicher, S.; Breitwieser, D.; Ribitsch, V.; Stana-Kleinschek, K.; Spirk, S. Design of anticoagulant surfaces based on cellulose nanocrystals. *Chem. Commun.* **2014**, *50*, 13070–13072.
- (28) Pubchem. <https://pubchem.ncbi.nlm.nih.gov> (accessed Mar 26, 2018).
- (29) Uhlig, M.; Fall, A.; Wellert, S.; Lehmann, M.; Prevost, S.; Wagberg, L.; von Klitzing, R.; Nystrom, G. Two-Dimensional Aggregation and Semidilute Ordering in Cellulose Nanocrystals. *Langmuir* **2016**, *32* (2), 442–450.
- (30) The Process Development Center. <https://umaine.edu/pdc> (accessed Mar 9, 2018).
- (31) Bartel, M.; Remde, H.; Bohn, A.; Ganster, J. Barrier properties of poly(lactic acid)/cloisite 30B composites and their relation to oxygen permeability and relative humidity. *J. Appl. Polym. Sci.* **2017**, *134*(5), DOI: 10.1002/app.44424.
- (32) Aulin, C.; Gällstedt, M.; Lindström, T. Oxygen and oil barrier properties of microfibrillated cellulose films and coatings. *Cellulose* **2010**, *17* (3), 559–574.
- (33) Rodionova, G.; Lenes, M.; Eriksen, O.; Gregersen, O. Surface chemical modification of microfibrillated cellulose: improvement of barrier properties for packaging applications. *Cellulose* **2011**, *18* (1), 127–134.
- (34) Bedane, A. H.; Eic, M.; Farmahini-Farahani, M.; Xiao, H. N. Water vapor transport properties of regenerated cellulose and nanofibrillated cellulose films. *J. Membr. Sci.* **2015**, *493*, 46–57.
- (35) Nair, S. S.; Zhu, J.; Deng, Y.; Ragauskas, A. J. High performance green barriers based on nanocellulose. *Sustainable Chem. Processes* **2014**, *2* (1), 23.
- (36) Bedane, A. H.; Eic, M.; Farmahini-Farahani, M.; Xiao, H. N. Theoretical modeling of water vapor transport in cellulose-based materials. *Cellulose* **2016**, *23* (3), 1537–1552.
- (37) Dalgleish, B. J.; Trumble, K. P.; Evans, A. G. The Strength and Fracture of Alumina Bonded with Aluminum-Alloys. *Acta Metall.* **1989**, *37* (7), 1923–1931.
- (38) Cao, H. C.; Thouless, M. D.; Evans, A. G. Residual-Stresses and Cracking in Brittle Solids Bonded with a Thin Ductile Layer. *Acta Metall.* **1988**, *36* (8), 2037–2046.
- (39) Schrenk, W. J.; Alfrey, T., Jr. Coextruded Multilayer Polymer Films and Sheets. In *Polymer Blends*; Paul, D. R., Ed.; Academic Press: Cambridge, Massachusetts, 1978.
- (40) Dooley, J.; Tung, H. *Coextrusion. Processing and Finishing of Polymeric Materials*; Wiley: Hoboken, New Jersey, 2011.
- (41) Youngblood, J.; Liu, J.; Moon, R. Mechanical and fracture behaviors of cellulose-based multilayer laminate. *Proceedings the Society of Engineering Science 51st Annual Technical Meeting*, West Lafayette, IN, October 1–3, 2014. Purdue University Libraries Scholarly Publishing Services: West Lafayette, IN, 2014.